Sub-Nyquist sampling method and its application in high-frequency electric-field measurement

Article *in* Optical Engineering · November 2019

DOI: 10.1117/1.OE.58.11.114106

5 authors, including:

Lyu Fangxing
Xi'an Jiaotong University
8 PUBLICATIONS **38** CITATIONS
SEE PROFILE

Chunyang Han
Xi'an Jiaotong University
27 PUBLICATIONS **143** CITATIONS
SEE PROFILE

Optical Engineering

OpticalEngineering.SPIEDigitalLibrary.org

Sub-Nyquist sampling method and its application in high-frequency electric-field measurement

Hui Ding
Fangxing Lyu
Haichen Zhao
Xu Niu
Chunyang Han

SPIE.

Hui Ding, Fangxing Lyu, Haichen Zhao, Xu Niu, Chunyang Han, "Sub-Nyquist sampling method and its application in high-frequency electric-field measurement," *Opt. Eng.* **58**(11), 114106 (2019), doi: 10.1117/1.OE.58.11.114106.

Sub-Nyquist sampling method and its application in high-frequency electric-field measurement

Hui Ding,[a] Fangxing Lyu,[a,b,*] Haichen Zhao,[a] Xu Niu,[a] and Chunyang Han[a]
[a]Xi'an Jiaotong University, State Key Laboratory of Electrical Insulation and Power Equipment, Xi'an, China
[b]Ankang University, School of Electronics and Information Engineering, Ankang, China

Abstract. A high-frequency signal sampling approach by combining with compressive sensing and random equivalent sampling technology is proposed. The proposed sampling method achieves ~10 times faster equivalent sampling rate by utilizing three parallel sub-Nyquist low-rate analog-to-digital converters (TPSL-ADC). By the union of the optical electric-field sensor with wide dynamic range and the proposed TPSL-ADC sampling method, a complete high-frequency electric-field signal measurement system has been realized. The high-frequency electric-field signal with an equivalent sampling rate of 1 GS/s is captured by utilizing three parallel ADCs with sampling rates of ~32.3, 31.3, and 30.3 MS/s, respectively. The effectiveness of the proposed electric-field sensing and detecting system has been experimentally demonstrated. [DOI: 10.1117/1.OE.58.11.114106]

Keywords: sub-Nyquist sampling; high-frequency electric-field measurement; compressive sensing.

Paper 190942 received Jul. 16, 2019; accepted for publication Nov. 11, 2019; published online Nov. 26, 2019.

1 Introduction

In the field of electromagnetic research, the technology of high-frequency electric-field measurement is an important way to reveal the characteristics of high-frequency electromagnetic field and evaluate the effectiveness of electromagnetic protection, etc.[1–4] Therefore, research on the technology of high-frequency electric-field measurement has become a key topic in the field of electromagnetic research.[5,6] For a high-frequency electric-field measurement system, not only is a high-performance sensor module needed but a high-frequency signal acquisition module also is necessary.[7,8] The common way of acquiring the high-frequency signal is utilizing a high-frequency oscilloscope, but it is not suitable for the establishment of a portable measurement system due to its bulky size and high cost.

For most of the high-frequency periodic measured signals, they usually consist of a relatively small number of narrow frequency components over a board spectrum range, so they are sparse in the Fourier domain.[9] In the acquisition of these sparse signals, compressive sensing (CS) is a promising solution to achieve high sampling rates with low-rate analog-to-digital converters (ADCs).[10–13] The idea of CS is that the spectral information of these sparse signals is much less than its bandwidth, so the original signal can be reconstructed from a small set of random projections. Usually, the CS-based method requires the premodulation of the original analog signal with a pseudorandom sequence at the Nyquist rate.[14,15] However, the implementation of such a pseudorandom sequence greatly raises the complexity of the system. In comparison, random equivalent sampling (RES) technology provides another attractive data sampling approach, which can reconstruct the high-frequency signal by utilizing low-rate ADC.[16–18] Specifically, RES reconstructs the original analog signal via multiple sampling at random positions by dithering the phase of the sampling clock. In order to rebuild the signal, the samples are realigned within a cycle of the signal after obtaining the time interval between the trigger signal and the rising edge of the sample clock. Therefore, both a triggering pulse signal as a stable reference and a high-accuracy circuit for the time interval measurement are required, and this will raise the complexity of the RES-based method.[19,20] Moreover, because of the randomness of the phase between the sampling and triggering pulse signal, many RES samples may be mapped to one sample in the realigned process, which causes the low-efficiency of the RES technology.

In this paper, a high-frequency signal sampling method combining CS and RES technology is proposed. We obtain the RES samples of the high-frequency original signal by three parallel sub-Nyquist low-rate analog-to-digital converters (TPSL-ADC) and reconstruct the high-frequency signal by a CS-based procedure. These three sub-ADCs are clocked at three different sub-Nyquist rates, which are pairwise coprime.[12,21] The data sampled by one of ADCs are a constant when the frequency of the measured signal is a multiple of one, the recovered signal may have multiple solutions if only by two sampling channels, so we require three sampling channels to collect enough information to recover the original signal instead of two channels. Compared with the other CS-enhanced RES methods, the attractive advantages of the proposed TPSL-ADC sampling method are that three ADCs work independently, and no additional circuitry is required. By the combination of the optical electric-field sensors with good dynamic performance,[22–24] we can achieve a high-frequency electric-field signal measurement system with the proposed TPSL-ADC sampling method. Experimental results show that the proposed electric-field measurement system achieves 1-GS/s equivalent sampling rate by employing three sub-ADCs with sampling rates of ~32.3, ~31.3, and ~30.3 MS/s, respectively. These results are very encouraging toward the development of a high-frequency electric-field measurement system in practical applications.

*Address all correspondence to Fangxing Lyu, E-mail: lfx85ilu@stu.xjtu.edu.cn

0091-3286/2019/$28.00

2 Theoretical Analysis and Numerical Simulation of the Proposed TPSL-ADC Sampling Method

2.1 *Sampling Architecture*

An illustrative scheme of the proposed TPSL-ADC sampling method is shown in Fig. 1, which consists of three parallel sampling channels (sub-ADC_1, sub-ADC_2, and sub-ADC_3). The sensor's high-frequency output temporal waveform $E_{\text{out}}(t)$ is concurrently sampled by three parallel low-rate sub-ADCs with the sampling rate far lower than the Nyquist rate. These three ADCs are clocked at different sub-Nyquist sample rates of f_e/N_1, f_e/N_2, and f_e/N_3 respectively, where f_e is the equivalent sampling rate. Parameters N_1, N_2, and N_3 are the ratios of equivalent sampling rate f_e to sub-Nyquist sample rates of three ADCs, respectively. Let $T_e = 1/f_e$ be the equivalent sampling interval, so the sampling intervals of three ADCs are N_1T_e, N_2T_e, and N_3T_e, respectively. Suppose N is the number of equivalent samples, M_1, M_2, and M_3 are the numbers of samples obtained from sub-ADC_1, sub-ADC_2, and sub-ADC_3, respectively. Let E_{out} denote the sampling sequence quantized at the equivalent sampling rate, which can be expressed as

$$E_{\text{out}}[m] = E_{\text{out}}(mT_e), \quad 1 \le m \le N. \tag{1}$$

Thus, the sampling sequences captured from three low-rate ADCs (sub-ADC_1, sub-ADC_2, and sub-ADC_3) E_1, E_2, and E_3 can be expressed as

$$\begin{cases} E_1[m] = E_{\text{out}}(mN_1T_e),\ 1 \le m \le M_1 \\ E_2[m] = E_{\text{out}}(mN_2T_e + \tau_{21}),\ 1 \le m \le M_2 \\ E_3[m] = E_{\text{out}}(mN_3T_e + \tau_{31}),\ 1 \le m \le M_3 \end{cases}, \tag{2}$$

where τ_{21} and τ_{31} are the start time differences from the first sampler, respectively.

After acquisition, these samples are resequenced into a set of sampling sequences E, namely $E = [E_1^{\text{T}}, E_2^{\text{T}}, E_3^{\text{T}}]^{\text{T}}$. E is the observation matrix, and E_{out} is the equivalent sample matrix. M_1, M_2, and M_3 are all integers, which are the largest integer smaller than N/N_1, N/N_2, N/N_3, respectively. Obviously, the proposed TPSL-ADC sampling method can obtain M ($M = M_1 + M_2 + M_3$) nonuniform samples in the sampling duration of NT_e.

It is doubtless that the proposed TPSL-ADC sampling module with coprime sampling rates can obtain more information than those with noncoprime sampling rates by the same average sampling rate.[12] Hence, N_1, N_2, and N_3 are all chosen to be coprime. In order to enhance the performance of the sub-Nyquist sampling module, N_1, N_2, and N_3 should be much bigger than 1. The larger N_1, N_2, and N_3 are, the lower the sampling rates of three ADCs are.

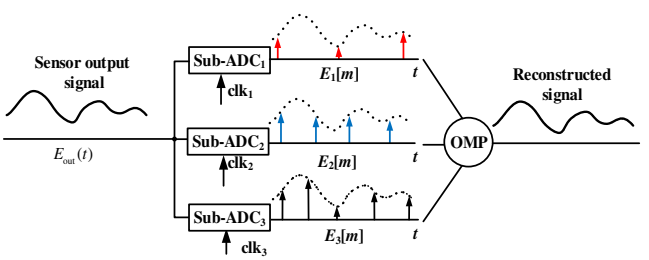

Fig. 1 Scheme of the proposed TPSL-ADC sapling method.

But larger N_1, N_2, and N_3 are at the price of larger sampling duration since enough samples are required to recover the signal. In the following simulation and experiment, the value of N is set as 1000. Therefore, we should choose appropriate values of N_1, N_2, and N_3, which are 31, 32, and 33 in our work.

2.2 *Measurement Matrix*

In order to reconstruct the high-frequency original signal with the CS theory, we need to construct a measurement matrix coincident with the proposed TPSL-ADC sampling method, which satisfies the restricted isometry property (RIP) condition. In this work, the measurement matrix can be constructed by the well-known Whittaker–Shannon interpolation formula, which has been demonstrated to satisfy the RIP condition.[13] According to the Whittaker–Shannon interpolation theory, the value at a given time t and the equivalent samples satisfy the following equation:

$$E_{\text{out}}(t) \approx \sum_{n=1}^{N} E_{\text{out}}(nT_e) \cdot \text{sinc}\left(\frac{t}{T_e} - n\right). \tag{3}$$

By inserting Eq. (3) into Eq. (2), we have

$$\begin{cases} E_1[m] \approx \sum_{n=1}^{N} E_{\text{out}}(nT_e) \cdot \text{sinc}\left(\frac{mN_1T_e}{T_e} - n\right), 1 \le m \le M_1 \\ E_2[m] \approx \sum_{n=1}^{N} E_{\text{out}}(nT_e) \cdot \text{sinc}\left(\frac{mN_2T_e + \tau_{21}}{T_e} - n\right), 1 \le m \le M_2 \\ E_3[m] \approx \sum_{n=1}^{N} E_{\text{out}}(nT_e) \cdot \text{sinc}\left(\frac{mN_3T_e + \tau_{31}}{T_e} - n\right), 1 \le m \le M_3 \end{cases}. \tag{4}$$

Furthermore, the relationship between the nonuniform sample of size M and the uniform equivalent samples of size N can be expressed by the following matrix–vector representation:

$$\begin{bmatrix} E_1[1] \\ E_1[2] \\ \vdots \\ E_1[M_1] \end{bmatrix} = \begin{bmatrix} \phi_{1,1} & \phi_{1,2} & \cdots & \phi_{1,N} \\ \phi_{2,1} & \phi_{2,2} & \cdots & \phi_{2,N} \\ \vdots & \vdots & \ddots & \vdots \\ \phi_{M_1,1} & \phi_{M_1,2} & \cdots & \phi_{M_1,N} \end{bmatrix} \begin{bmatrix} E_{\text{out}}[T_e] \\ E_{\text{out}}[2T_e] \\ \vdots \\ E_{\text{out}}[NT_e] \end{bmatrix},$$

$$\begin{bmatrix} E_2[1] \\ E_2[2] \\ \vdots \\ E_2[M_2] \end{bmatrix} = \begin{bmatrix} \varphi_{1,1} & \varphi_{1,2} & \cdots & \varphi_{1,N} \\ \varphi_{2,1} & \varphi_{2,2} & \cdots & \varphi_{2,N} \\ \vdots & \vdots & \ddots & \vdots \\ \varphi_{M_2,1} & \varphi_{M_2,2} & \cdots & \varphi_{M_2,N} \end{bmatrix} \begin{bmatrix} E_{\text{out}}[T_e] \\ E_{\text{out}}[2T_e] \\ \vdots \\ E_{\text{out}}[NT_e] \end{bmatrix},$$

$$\begin{bmatrix} E_3[1] \\ E_3[2] \\ \vdots \\ E_3[M_3] \end{bmatrix} = \begin{bmatrix} \gamma_{1,1} & \gamma_{1,2} & \cdots & \gamma_{1,N} \\ \gamma_{2,1} & \gamma_{2,2} & \cdots & \gamma_{2,N} \\ \vdots & \vdots & \ddots & \vdots \\ \gamma_{M_3,1} & \gamma_{M_3,2} & \cdots & \gamma_{M_3,N} \end{bmatrix} \begin{bmatrix} E_{\text{out}}[T_e] \\ E_{\text{out}}[2T_e] \\ \vdots \\ E_{\text{out}}[NT_e] \end{bmatrix}, \tag{5}$$

where ϕ, φ, and γ are the matrixes motivated by three low-rate sub-ADCs, respectively. According to Eq. (4), we can find that these matrixes can be expressed as

$$\begin{cases} \phi(m,n) = \mathrm{sinc}\left(\frac{mN_1T_e}{T_e} - n\right), 1 \le m \le M_1, 1 \le n \le N \\ \varphi(m,n) = \mathrm{sinc}\left(\frac{mN_2T_e+\tau_{21}}{T_e} - n\right), 1 \le m \le M_2, 1 \le n \le N \\ \gamma(m,n) = \mathrm{sinc}\left(\frac{mN_1T_e+\tau_{31}}{T_e} - n\right), 1 \le m \le M_3, 1 \le n \le N \end{cases}. \tag{6}$$

As shown in Eq. (6), the time differences τ_{21} and τ_{31} are an indispensable part of the measurement matrixes, which plays an important role in the recovery process. In practical applications, the start time differences τ_{21} and τ_{31} with the first sampler distributes in the time intervals of $[0, N_2T_e]$ and $[0, N_3T_e]$, and we should quantize them into integers divided by T_e. Usually, the start time differences τ_{21} and τ_{31} are measured by a time-to-digital circuitry (TDC), but TDC would increase the complexity of the system. In our work, the clock signals of three sub-ADCs generated by the FPGA system board are not synchronous, but the start time differences τ_{21} and τ_{31} are fixed. The start time differences τ_{21} and τ_{31} can be obtained through the hypothetical test method. If the assumed time differences τ_{21} and τ_{31} coincide with the true value, the spectrum of the reconstructed signal is in accordance with that of the original waveform.

Consequently, we can construct the measurement matrix $\mathbf{\Phi}$ with the obtained τ_{21} and τ_{31}, which can be expressed as

$$\mathbf{\Phi} = [\phi^{\mathrm{T}}, \varphi^{\mathrm{T}}, \gamma^{\mathrm{T}}]^{\mathrm{T}}. \tag{7}$$

2.3 *Signal Recovering Algorithm*

From Eq. (5), the observation matrix E from three sub-ADCs and the equivalent sample matrix E_{out} can be further expressed as

$$E = \mathbf{\Phi} \cdot E_{\mathrm{out}}. \tag{8}$$

As given in Eq. (8), the dimension of E is often much lower than that of E_{out} ($M \ll N$). Therefore, reconstructing E_{out} from E is an ill-posed problem, and there may be many possible solutions of Eq. (8). As a high-frequency periodic signal, E_{out} can be sparsely represented in the form of Fourier transform, so we have

$$E_{\mathrm{out}} = \mathbf{\Psi} \cdot \mathbf{X}. \tag{9}$$

Here, $\mathbf{\Psi}$ is the Fourier basis matrix, which can be expressed as

$$\mathbf{\Psi} = \frac{1}{\sqrt{N}} \begin{bmatrix} 1 & 1 & \cdots & 1 \\ 1 & e^{j2\pi/N} & \cdots & e^{j2\pi\times(N-1)/N} \\ 1 & e^{j2\pi\times2/N} & \cdots & e^{j2\pi\times2\times(N-1)/N} \\ \vdots & \vdots & \ddots & \vdots \\ 1 & e^{j2\pi\times(N-1)/N} & \cdots & e^{j2\pi\times(N-1)\times(N-1)/N} \end{bmatrix}, \tag{10}$$

$\mathbf{X}$ is the sparse Fourier coefficient of E_{out} in $\mathbf{\Psi}$. Therefore, Eq. (8) can be rewritten as

$$E = \mathbf{\Phi} \cdot \mathbf{\Psi} \cdot \mathbf{X} = \mathbf{A} \cdot \mathbf{X}, \tag{11}$$

where $\mathbf{A} = \mathbf{\Phi} \cdot \mathbf{\Psi}$ is the sensing matrix. The purpose of this CS-based signal recovering algorithm is to find the sparsest solution of $\mathbf{X}$ that contains the minimum number of nonzero Fourier coefficients in Eq. (11). However, the energy of one Fourier component would "leak" to other components due to the limited sampling length of the signal in time domain, the number of nonzero Fourier coefficient would greatly increase. In our work, we extend the dimension of the Fourier basis matrix from $N \times N$ to $N \times 5N$, which is equivalent to increasing the number of sampling points. Therefore, it can improve the resolution of the spectrum and reduce the negative impact of spectral leakage. An antileakage Fourier transform (ALFT) algorithm is applied to reconstruct the signal, which can be illustrated as follows:

Definition: $\mathbf{u}$ denotes the correlation coefficient matrix, $\mathbf{r}$ denotes the residual vector, i represents the iteration times, $\mathbf{s}_i$ represents the index set at the i'th iteration, $\mathbf{B}_i$ denotes the column set of sensing matrix $\mathbf{A}$ corresponding to $\mathbf{s}_i$, and λ represents the foot mark value corresponding to the selected column vector of $\mathbf{A}$.

Input: The sensing matrix $\mathbf{A}$, the observation matrix E from three sub-ADCs, the relative error ε.

Output: The approximation $\mathbf{X}^{\#}$ of $\mathbf{X}$.

Step 1. Initialize the index set $\mathbf{s}_0$, the column set $\mathbf{B_0}$, and the approximation $\mathbf{X}^{\#}$ to an empty set, and the residual $\mathbf{r}$ to E. Normalize every column vector of $\mathbf{A}$. Set a predetermined threshold relative error $\varepsilon = 4 * 10^{-2}$, the number of iterations $i = 1$.

Step 2. Compute the correlation coefficient matrix $\mathbf{u}$ of the column of sensing matrix $\mathbf{A}$ and the residual $\mathbf{r}$ using

$$\mathbf{u} = \left\{ \mathbf{u_j} \middle| \mathbf{u_j} = \frac{\langle \mathbf{A_j^T}, \mathbf{r} \rangle}{\|\mathbf{A_j^T}\| \|\mathbf{r}\|} \middle| \mathbf{j} = 1,2,\ldots,5\mathbf{N} \right\}, \tag{12}$$

where $\mathbf{A_j}$ is the column vector of $\mathbf{A}$, $\mathbf{A_j^T}$ is the transpose matrix of $\mathbf{A_j}$, $\langle \mathbf{A_j^T}, \mathbf{r} \rangle$ is the inner product of $\mathbf{A_j^T}$ and r, and $\| \cdot \|$ is the Euclidean norm of the vector. Since $\mathbf{A_j^T}$ has been normalized ($\|\mathbf{A_j^T}\| = 1$) and $\|\mathbf{r}\|$ is identical at each iteration, Eq. (12) can be simply expressed as

$$\mathbf{u} = \{ \mathbf{u_j} | \mathbf{u_j} = \langle \mathbf{A_j^T}, \mathbf{r} \rangle | \mathbf{j} = 1,2,\ldots,5\mathbf{N} \}. \tag{13}$$

Step 3. Select the largest correlation coefficient, store the corresponding foot mark to λ, and update the index set $\mathbf{s_i}$, i.e., $\mathbf{s_i} = \mathbf{s_{i-1}} \cup \{\lambda\}$. Then renew the column set $\mathbf{B}_i$ by the union of the corresponding column of sensing matrix $\mathbf{A}$, i.e., $\mathbf{B_i} = [\mathbf{B_{i-1}}, \mathbf{A_\lambda}]$, and set the corresponding column vector $\mathbf{A_\lambda}$ to 0.

Step 4. Calculate the contribution of the existing Fourier components by the least square method [Eq. (14)], i.e.,

$$\mathbf{X}^{\#} = (\mathbf{B_i^T B_i})^{-1} \mathbf{B_i^T r}. \tag{14}$$

Update $\mathbf{r}$ by subtracting the contribution of selected coefficient

$$\mathbf{r} = \mathbf{E} - \mathbf{B_i X}^{\#}. \tag{15}$$

Step 5. Repeat steps 2 to 4 until the Euclidean norm of the updated residual $\mathbf{r}$ meets a predetermined threshold ε.

In this way, we can obtain the approximation $\mathbf{X}^{\#}$ of $\mathbf{X}$ and reconstruct the signal E_{out} through Eq. (9).

2.4 *Numerical Simulation*

In our simulation, a high-frequency signal is used to demonstrate the proposed TPSL-ADC sampling method, which can be defined as

$$E_{\text{out}}(t) = \sum_{i=1}^{K} E_i \cos(2\pi f_i t - p_i), \tag{16}$$

where K is the number of nonzero frequency components, E_i, f_i, and p_i are the amplitude, frequency, and the phase of each component, respectively. K is set as 5, E_i is randomly chosen in [0.1, 1], f_i is randomly chosen in [0.1, 20] GHz, and p_i is randomly chosen in $[-\pi, \pi]$. The start time differences τ_{21} and τ_{31} are randomly chosen in $[0, N_2]$ and $[0, N_3]$, respectively. Without loss of generality, the values of E_1, E_2, E_3, E_4, and E_5 are randomly set as 0.2, 1, 0.8, 0.2, and 0.9. f_1, f_2, f_3, f_4, and f_5 are randomly set as 5.458143066, 5.685463435, 14.34794244, 3.700895987, and 16.67573014 GHz, whereas p_1, p_2, p_3, p_4, and p_5 are randomly set as $\pi/12$, $\pi/4$, $-\pi/6$, $\pi/3$, and $-\pi/5$, respectively. τ_{21} and τ_{31} are randomly set as 3 and 11, respectively.

The values of N_1, N_2, and N_3 are 31, 32, and 33, and the sampling rates of sub-ADCs are $f_1 = f_e/31$, $f_2 = f_e/32$, and $f_3 = f_e/33$, respectively. In our simulation, the equivalent sampling rate of the reconstructed signal is $f_e = 100$ GS/s, so the sampling rates of sub-ADCs are $f_1 \approx 3.23$ GS/s, $f_2 \approx 3.13$ GS/s, and $f_3 \approx 3.03$ GS/s, respectively. The total number of the reconstructed signal is $N = 1000$, so the sampling number of sub-ADC1, sub-ADC2, and sub-ADC3 (M_1, M_2, and M_3) are 33, 32, and 31, respectively.

First, according to Eq. (1), three sampling sequences are captured by three sub-Nyquist ADCs. The RES samples of size M is shown in Fig. 2(a), and its locally enlarged images are shown in Fig. 2(b). The Fourier basis matrix $\mathbf{\Psi}$ is available, and the measurement matrix Φ would be constructed by using Eq. (6). Then, we reconstruct the signal by the proposed algorithm illustrated in Sec. 2.3. The correlation coefficient would be computed in step 2. Next, in step 3, we select the largest coefficient and renew the column set B_i. The correlation coefficient is updated by subtracting the contribution of the selected components in step 4. This procedure uses the updated data as the input of the new iteration until the approximation relative error of $\mathbf{E}$ meets a predetermined threshold ε, which is shown in Fig. 3. At last, the approximation $\mathbf{X}^{\#}$ of $\mathbf{X}$ would be achieved to reconstruct the signal.

Figure 4 shows the waveform of the reconstructed and original signal in a period of time, respectively. As shown in Fig. 4, the time interval between two adjacent points of the reconstructed signal is 10^{-11} s, which means that the equivalent sampling rate of 100 GS/s has been achieved through the proposed sampling method. The sum sampling rate of three sub-Nyquist ADCs is ~9.39 GS/s, which is lower than 1/10th of the equivalent sampling rate of the reconstructed signal. Moreover, the reconstructed waveform

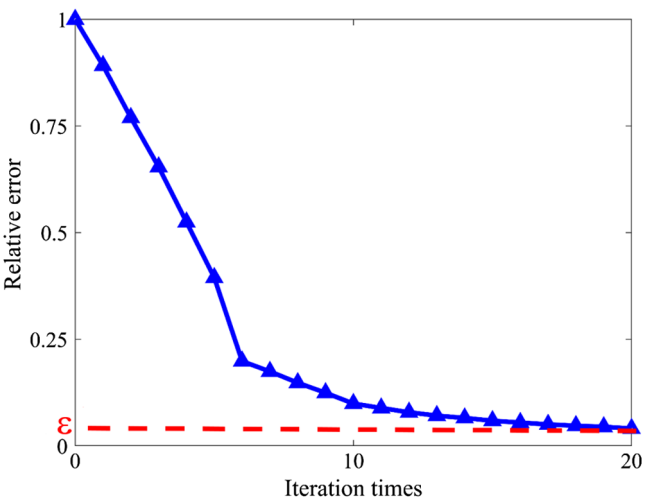

Fig. 3 The change of relative error ε with the iteration times.

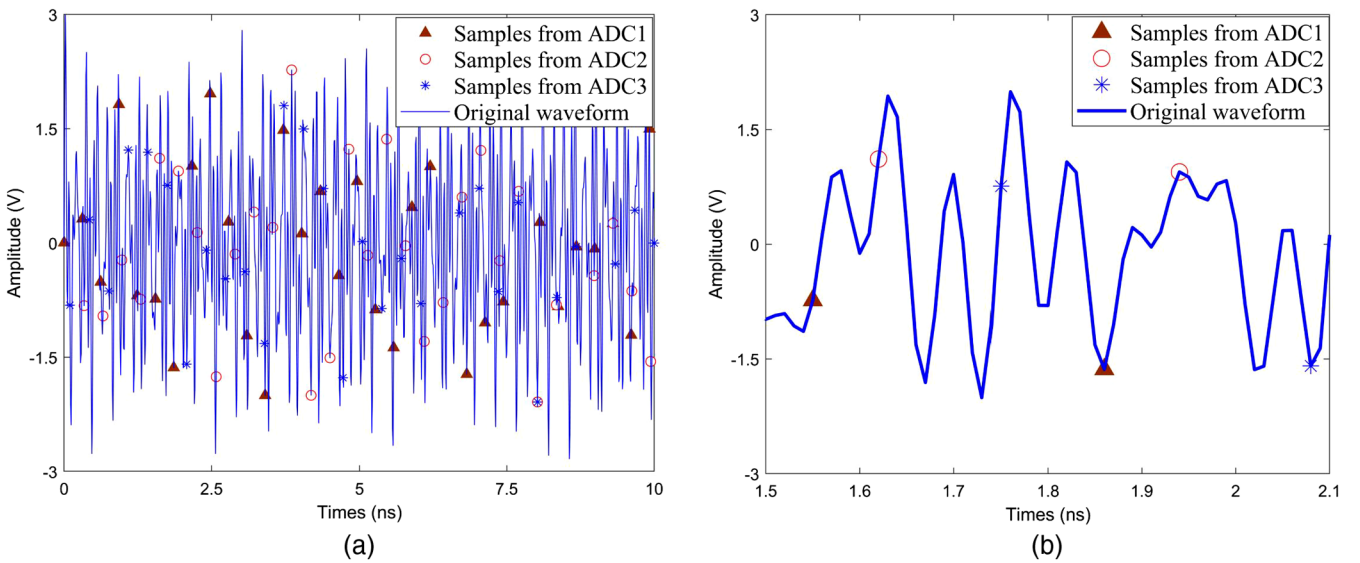

Fig. 2 (a) Samples captured by three low-rate ADCs from the original signal. (b) Locally enlarged images of (a) in a period of time.

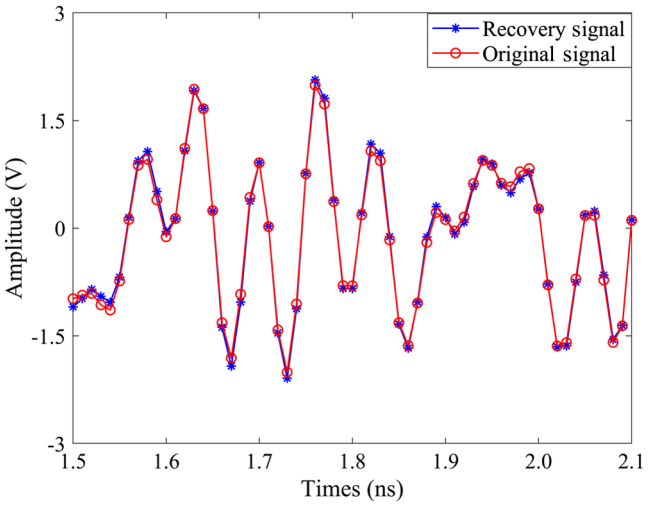

Fig. 4 Reconstructed waveform by the proposed sub-Nyquist sampling method and the corresponding original waveform over a period of time.

is well coincident with the original waveform. The quality of the reconstructed signal is evaluated by signal-to-noise ratio (SNR), which can be defined as

$$\mathrm{SNR} = 20 \cdot \log_{10} \frac{\|E_{\mathrm{out}}\|}{\|E_{\mathrm{out}} - E_{\mathrm{new}}\|}, \tag{17}$$

where E_{new} is the reconstructed signal, $\|\cdot\|$ is the Euclidean norm. The SNR of the reconstructed signal is calculated to be 59.5 dB, which means that original signal is well recovered. After replacing all the random values in Eq. (15) and reconstructing the corresponding signal, we can obtain that the mean of the SNR values over 100 times is 57.03 dB. Therefore, the feasibility of the proposed TPSL-ADC sampling method has been demonstrated.

Also, we assess the effect of Gaussian noise on the quality of the reconstructed signal. When the noise of the original signal increases from 10 to 70 dB, the mean of the SNR values under each noise condition are shown in Fig. 5. As shown in Fig. 5, even when the noise is very high (such as the input SNR of signal is 10 dB), we can still recover the original signal very well. This proves that the proposed TPSL-ADC sampling method has good performance against Gaussian noise.

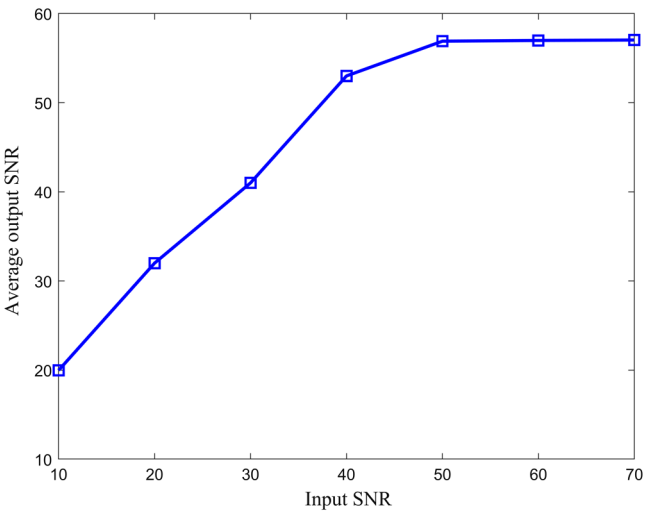

Fig. 5 The average SNR of reconstructed signal in the different noise levels.

3 Experiments and Discussions

3.1 *System Principle of the High-Frequency Electric-Field Sensing and Detecting System*

The proposed TPSL-ADC sampling method provides a new approach to detect the high-frequency signal with three low-rate ADCs. Benefiting from the good dynamic performance of optical electric-field sensors, we can realize a high-frequency electric-field sensing and detecting system by the union of the proposed sub-Nyquist sampling method. The operational principle of the high-frequency electric-field sensing and detecting system is shown in Fig. 6. A beam propagates into an optical electric-field sensor, and the sensor output electric signal is modulated by the applied electric-field signal. Then, the high-frequency output signal can be detected by three low-rate sub-ADCs in the sub-Nyquist sampling module.

3.2 *Experimental Setup*

A proof-of-concept experiment is carried out to demonstrate the proposed high-frequency electric-field sensing and detecting system. The experimental setup is shown in Fig. 7. It mainly consists of a laser (TSL510, Santec), a homemade optical electric-field sensor, a function generator (DSG3000, RIGOL), a high-voltage power amplifier, a transverse electromagnetic (TEM) cell, a photodetector (PD, Thorlabs, PDB150C), three ADCs (AD9226, AD), an FPGA system board (EP4CE10F18N, Altera), a computer with Matlab software, an oscilloscope (DSO9254A, Agilent), etc. Light from the laser launches into an optical electric-field sensor and is collected at the output. The electric-field signal is generated by the arbitrary function generator and boosted by a high-voltage power amplifier. When a high-frequency electric-field is applied to the sensor by a TEM cell, the corresponding output signal of the sensor is modulated by the applied electric-field signal. Then, the output signal is concurrently sampled by three parallel low-rate sub-ADCs, and the original signal is reconstructed by the proposed sub-Nyquist sampling module. Simultaneously, the signal is also collected by a high-speed oscilloscope as the reference signal to evaluate the reconstructed signal.

The optical electric-field sensor applied to this system is based on the electro-optic (EO) effect of the $LiNbO_3$ crystal. As shown in Fig. 8, inside the sensor head, the beam passes through a polarizer, a quarter-wave plate, a $LiNbO_3$ crystal, and a polarization state analyzer. The sensor output is modulated by the applied electric-field signal through the polarization state analyzer. As the miniature fiber optics and

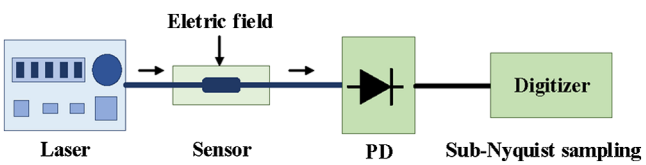

Fig. 6 Schematic configuration of the proposed high-frequency electric-field measurement system. PD, photodetector.

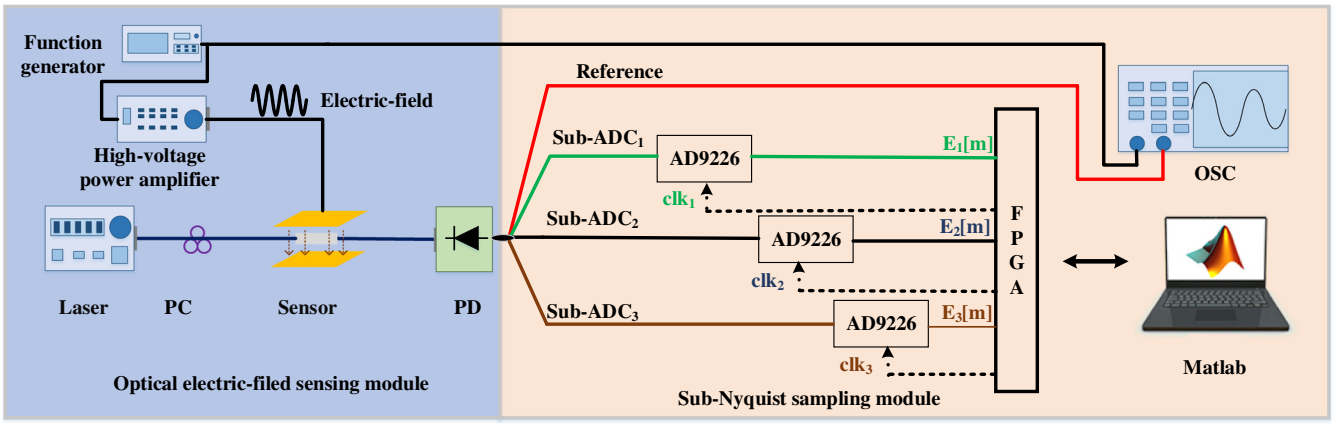

Fig. 7 Experimental setup of the proposed high-frequency electric-field sensing and detecting system. PC, polarization controller; PD, photodetector; OSC, oscilloscope.

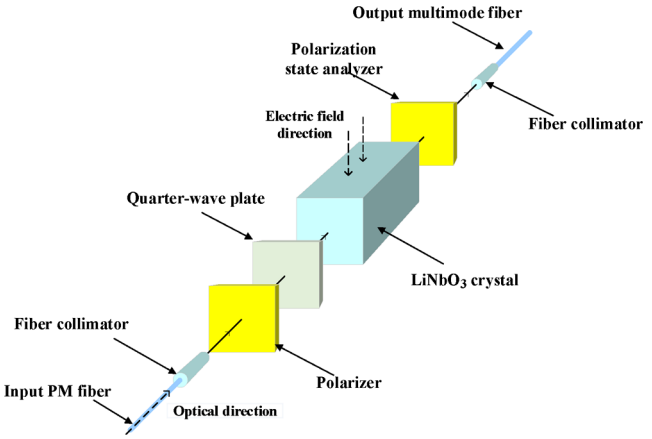

Fig. 8 The structure of the optical electric-field sensor. PM fiber, polarization maintaining fiber.

fast EO effect, the optical electric-field sensor can be very small in size and have large intrinsic bandwidths. Hence, the sensor is suitable to verify the feasibility of the proposed high-frequency electric-field sensing and detecting system.

In the sub-Nyquist sampling module, the fixed clock signals of three sub-ADCs are generated by the FPGA system board. The maximum sampling rate of ADC (AD9226) can reach 65 MS/s, and the full-power bandwidth is 780 MHz. Due to the limitation of the performance of the FPGA and ADC, the equivalent sampling rate of the reconstructed signal adopted to verify the proposed sampling method is $f_e = 1$ GS/s. So the sampling rates of three sub-ADCs are $f_1 = f_e/31 \approx 32.3$ MS/s, $f_2 = f_e/32 \approx 31.3$ MS/s, and $f_3 = f_e/33 \approx 30.3$ MS/s, respectively. The frequency of the applied electric-field signal is limited to 200 MHz.

3.3 *Experiment and Discussion*

First, by employing a standard single-tone test signal with the frequency at 100 MHz to the input of the TPSL-ADC sampling module, we can obtain the start time differences τ_{21} and τ_{31} by comparing the spectra of the original and

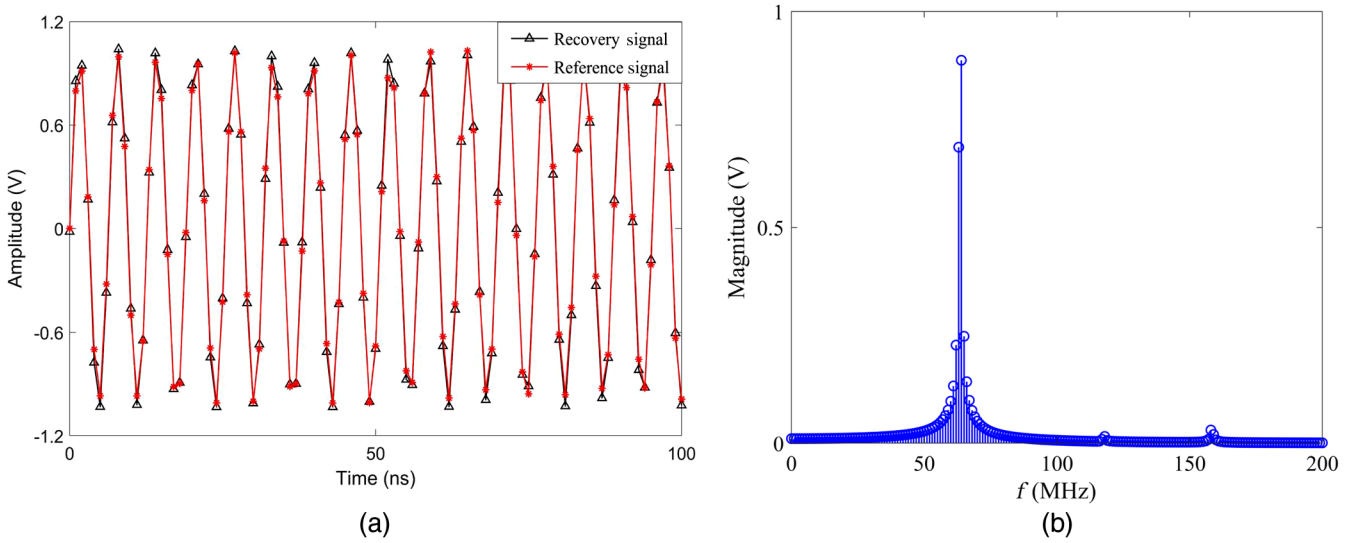

Fig. 9 (a) Reconstructed waveform by using the proposed high-frequency electric-field measurement system and corresponding reference waveform recorded by OSC. (b) The Fourier spectrum of the reccovery signal.

reconstructed signal with different τ_{21} and τ_{31}. The values of τ_{21} and τ_{31} are equal to 5 and 12 in our experiments, respectively.

Then, the electric-field signals are applied to the optical electric-field sensor, and the sensor output high-frequency signal is detected by the proposed TPSL-ADC sampling module. After the fixed numbers of acquisition runs, a low-rate RES sampling sequence is obtained and used to reconstruct the sensor output waveform by adopting the proposed ALFT procedure. The intensity of applied electric-field is 0.5 kV/m, and the frequency of applied electric-field is ranging from 10 to 200 MHz. A typical response waveform and Fourier spectrum reconstructed by the proposed sub-Nyquist sampling method are shown in Fig. 9. As shown in Fig. 9(a), we can see that the reconstructed signal well coincides with the reference signal recorded by the OSC. The amplitude and frequency of the reconstructed signal are ∼1.25 V and ∼63.5 MHz. Moreover, the average SNR of the reconstructed signal is calculated to be 48.3 dB over 100 trails. The time interval between two adjacent points of the reconstructed signal is 10^{-9} s, which means that the equivalent sampling rate of 1 GS/s has been achieved. The sampling rates of three sub-ADCs are ∼32.3, ∼31.3, and ∼30.3 MS/s, respectively, so the sum sampling rate of three low speed ADCs is 93.9 MS/s and the ratio of the equivalent sampling rate to the sum sampling rate is larger than 10. This is consistent with the previous simulation result.

4 Conclusion

In conclusion, a high-frequency signal sampling approach is demonstrated based on three low-rate sampling ADCs by CS and RES technology. The high-frequency signal can be detected through properly selecting the sampling rates of three sub-Nyquist ADCs. Simulations show that the proposed sampling method can achieve the equivalent sampling rate of 100 GS/s by three sub-ADCs with sampling rates of ∼3.23, ∼3.13, and ∼3.03 GS/s. By the union of an optical electric-field sensor, a proof-of-concept experiment is carried out to demonstrate that the high-frequency electric-field signal can be well reconstructed. The ratio of the equivalent sampling rate to the average sampling rate is larger than 10, which will play a great role in the high-frequency electric-field measurement.

Acknowledgments

This work was supported by the National Natural Science Foundation of China under Contract Nos. 51377125 and 51777150, and Young Talent Fund of University Association for Science and Technology in Shaanxi. The authors have declared that no competing interests exist. Scientific Research Program funded by Shaanxi Provincial Education Department.

References

1. M. Bieler et al., "Ultrafast electric field measurements in semiconductors by spectral integration over electric field-induced Franz–Keldysh oscillations," *Appl. Phys. Lett.* **87**(4), 042102 (2005).
2. C. Han et al., "Silica microwire-based interferometric electric field sensor," *Opt. Lett.* **40**(16), 3683–3686 (2015).
3. T. Pfeifer et al., "Optoelectronic on chip characterization of ultrafast electric devices: measurement techniques and applications," *IEEE J. Sel. Top. Quantum Electron* **2**(3), 586–604 (1996).
4. M. S. Simeni et al., "Electric field measurements in a nanosecond pulse discharge in atmospheric air," *J. Phys. D Appl. Phys.* **50**(18), 184002 (2017).
5. C. Suo et al., "GIS very fast transients overvoltage testing using electric field measurements," *Integr. Ferroelectr.* **178**(1), 23–34 (2017).
6. S. J. Evan and A. V. Peterchev, "Electric field measurement of two commercial active/sham coils for transcranial magnetic stimulation," *J. Neural Eng.* **15**(5), 054001 (2018).
7. S. Sun et al., "A high-speed electrical impedance measurement circuit based on information-filtering demodulation," *Meas. Sci. Technol.* **25**(7), 075010 (2014).
8. M. Skold et al., "Quasi-real-time optical sampling scheme for high-speed signal acquisition and processing," *IEEE Photonic Technol. Lett.* **25**(5), 504–507 (2013).
9. D. Malioutov, M. Cetin, and A. S. Willsky, "A sparse signal reconstruction perspective for source localization with sensor arrays," *IEEE Trans. Signal Process.* **53**(8), 3010–3022 (2005).
10. D. L. Donoho, "Compressed sensing," *IEEE Trans. Inf. Theory* **52**(4), 1289–1306 (2006).
11. S. Kirolos et al., "Analog-to-information conversion via random demodulation," in *IEEE Dallas/CAS Workshop Des., Appl., Integr. and Software*, pp. 71–74 (2006).
12. Y. Zhao and S. Xiao, "Sparse multiband signal spectrum sensing with asynchronous coprime sampling," *Cluster Comput.* **22**(2), 4693–4702 (2019).
13. Y. Zhao, Y. Hu, and H. Wang, "Enhanced random equivalent sampling based on compressed sensing," *IEEE Trans. Instrum. Meas.* **61**(3), 579–586 (2012).
14. S. Qaisar et al., "Compressive sensing: from theory to applications, a survey," *J. Commun. Networks* **15**(5), 443–456 (2013).
15. L. Bai and S. Roy, "Compressive spectrum sensing using a bandpass sampling architecture," *IEEE J. Emerg. Sel. Top. Circuits Syst.* **2**(3), 433–442 (2012).
16. D. Qiu et al., "Design and implementation of 500 GSPS random equivalent sampling," in *12th IEEE Int. Conf. Electron. Meas. and Instrum.*, Vol. 2, pp. 953–957 (2015).
17. M. J. Shi, H. Zhang, and H. E. Dao-Qing, "Implementation of new random equivalent sampling technology," *Instrum. Tech. Sens.* **7**, 108–110 (2010).
18. V. N. Vyukhin, "Equivalent-time sampling and real-time digital oscillography interpolation optoelectronics," *Instrum. Data Process.* **44**(3), 228–231 (2008).
19. R. Z. Bhatti, M. Denneau, and J. Draper, "Phase measurement and adjustment of digital signals using random sampling technique," in *IEEE Int. Symp. Circuits and Syst.* (2006).
20. M. Strackx et al., "Analysis of a digital UWB receiver for biomedical applications using equivalent-time sampling," in *8th Eur. Radar Conf.*, pp. 206–209 (2011).
21. S. Huang et al., "Frequency estimation of multiple sinusoids with three sub-Nyquist channels," *Signal Process.* **139**, 96–101 (2017).
22. M. A. Al-Tarawni et al., "Improvement of integrated electric field sensor based on hybrid segmented slot waveguide," *Opt. Eng.* **56**(10), 107105 (2017).
23. L. Liu et al., "Analysis on the optimization of high frequency performance for optical voltage sensors based on Pockels effect," *IEEE Sens. J.* **17**(15), 4826–4833 (2017).
24. S. Bao et al., "Integrated optical electric field sensor from 10 kHz to 18 GHz," *IEEE Photonics Technol. Lett.* **24**(13), 1106–1108 (2012).

Hui Ding is a professor at Xi'an Jiaotong University. She received her PhD in measurement and instrumentation from Xi'an Jiaotong University, Xi'an, China, in 2004. Her current research interests include optical fiber sensing technology, optical information detection technology, ultrafast electromagnetic pulse measurement technology, and photonics ADC technology.

Fangxing Lyu is a PhD candidate at Xi'an Jiaotong University and a lecturer at Ankang University. He received his BS and MS degrees in measurement and instrumentation both from Xi'an Jiaotong University, Xi'an, China, in 2007 and 2010, respectively. His current research interests include optical fiber sensing technology and photonics ADC technology.

Haichen Zhao is an ME candidate at Xi'an Jiaotong University.

Xu Niu is an ME candidate at Xi'an Jiaotong University.

Chunyang Han is a postdoctor at Xi'an Jiaotong University. He received his PhD in measurement and instrumentation from Xi'an Jiaotong University, Xi'an, China, in 2018. He received his MS degree in controlling engineering from Central South University, Changsha, China, in 2011. His current research interests include optical fiber sensing technology and optical information detection technology.